Laser Engineered Graphene Paper for Mass Spectrometry Imaging

Kun Qian[1], Liang Zhou[1], Jian Liu[1], Jie Yang[1], Hongyi Xu[2], Meihua Yu[1], Amanda Nouwens[1,3], Jin Zou[2], Michael J. Monteiro[1] & Chengzhong Yu[1]

[1]Australian Institute for Bioengineering and Nanotechnology, [2]Materials Engineering and Centre for Microscopy and Microanalysis, [3]School of Chemistry and Molecular Biosciences, the University of Queensland, Brisbane, QLD 4072, Australia.

A pulsed laser engineering approach is developed to prepare novel functional graphene paper with graphitic nanospheres homogeneously decorated on the surface and the superior performance of engineered paper is revealed in matrix-free mass spectrometry (MS) detection and imaging. We demonstrate that the stability of graphene paper under intense irradiation can be dramatically increased through a designed laser engineering process by forming densely packed graphitic nanospheres on the paper surface. Moreover, the surface hydrophobicity is enhanced and electric conductivity is improved. The engineered graphene paper can image the invisible micro-patterns of trace amount molecules and increases the detection limit towards diverse molecules by over two orders of magnitude compared to the pristine graphene paper and commercial products in MS analysis.

Graphene materials are rapidly attracting interest due to their unique properties and widely spread applications[1–4]. With recent advances in nanotechnology, various nano-structured materials have been used in irradiation involved area, such as sensitive analysis of molecules[5–7], including graphene based nano-materials[8–15]. Nevertheless, graphene is not stable under strong irradiation conditions[4,16–20]. For example, the *in situ* formation of C_{60} on the surface of graphene under 80 keV electron beam irradiation was observed by Chuvilin et al.[17], and carbon clusters with larger sizes (C_n, n < 500) were also observed in the mass spectrometry (MS) spectra of graphene with high intensity during the laser desorption/ionization (LDI) process[19], which may decrease the detection sensitivity in MS based analysis. Considering the fact that carbon clusters produced from graphene during irradiation may have lower atomic energy (~ -0.26 eV/atom) and thus are more stable compared to graphene[17], we hypothesise that by introducing stable carbon species homogenously distributed on the surface *in situ*, engineered graphene products can meet the needs of applications designed in extreme conditions, e. g. intense irradiation.

As one of the key fields that require strong (laser) irradiation in nature, MS detection and imaging techniques, such as matrix assisted laser desorption/ionization (MALDI) MS, can help to visualise the spatial distribution of molecules without purification, extraction, separation, or labelling of bio-samples, which are important in early stage disease diagnosis and forensic applications[21,22]. Despite the substantial progress, the application of MALDI MS towards small molecules is limited because the matrices (normally small organo molecules like α-cyano-4-hydroxycinnamic acid, CHCA) introduce significant background signals during laser ablation in the low molecular range (<1000 Da). In addition, the large and irregular sizes of the matrix crystals (>10 µm) and sweet-spot effects limit the imaging spatial resolution and detection efficiency[5,6]. To date, overcoming the low sensitivity of MS based imaging towards small molecules and the preparation of stable functional materials under irradiation represent the key challenges to the field.

To address the above challenges, matrix-free MS techniques have been developed[5–15,23]. Secondary ion MS (SIMS) was one of the first matrix-free approaches used to detect and image molecules from biological samples using a high-energy primary ion beam to desorb and generate secondary ions from a surface[24,25]. For matrix free MS detection and imaging applications, an ideal substrate should have the following attributes: (1) stable with minimum matrix interference; (2) able to provide sufficient surface area and desirable interaction with analyte molecules; (3) electric conductive with high electron mobility and efficient in laser absorbance for desorption/ionization; and (4) homogeneous in surface for reproducibility and faithful replication of imaging[5,6,18]. However, currently used substrates are far from ideal and new materials with improved performance are in urgent demand.

Recently it was found that the functional sites on engineered graphene induced by laser irradiation could be utilized for enhanced electric capacitance[2,3]. In this study, we demonstrate that the stability of graphene paper

during intense laser irradiation can be dramatically increased through a pulsed-laser engineering process by forming densely packed graphitic nanospheres (stable under 300 keV electron beam) on the paper surface. Moreover, the surface hydrophobicity is enhanced and the electric conductivity is improved. The engineered graphene paper as a substrate for matrix-free LDI MS detection and imaging helps recognize invisible stamped micro-patterns, increasing the detection limit towards diverse molecules by over two orders of magnitude compared to the pristine graphene paper and commercial products. To our knowledge, the laser engineering approach represents a novel strategy compared to previous reports where the laser treatment was used either in a different manner or for other applications (see Table S1 for more details).

Results

The graphene sheets prepared by chemical reduction of graphene oxide were utilised as the precursor (Figure S1). The graphene paper was obtained by vacuum filtration of the as-synthesised graphene suspension (Figure 1a and 1b). A pulsed nitrogen laser with a wavelength of 337 nm was employed to engineer the graphene paper (Figure 1c). The laser beam scanning (~30 μm in spot diameter, 500 pulses for each spot) was programmed with the spot-to-spot distance of 30 μm in two dimensions to ensure the maximum and homogenous modification on the surface, which is also sufficient for the identification of latent fingerprints with a typical spatial resolution of 150 μm[22]. The laser energy was approximately 121.8 μJ for 100% laser intensity, which was adjusted to be 10%, 30% and 50% to study its influence on the structure and performance of engineered graphene papers (graphene paper was damaged by severe fragmentation at 80% intensity, data not shown). As shown in the digital image (Figure 1d), the engineered area of the graphene paper turns to dark black after laser treatment with 50% laser intensity. The engineered graphene paper is freestanding and highly flexible, which can be bent and twisted into large angles without breaking as displayed in the inset of Figure 1e. Consequently, the engineered graphene paper (1.5 cm × 0.75 cm) can be easily integrated on the top of a glass slide (Figure 1e) and used as a substrate for MS detection and imaging applications (Figure 1f).

The morphology of the engineered graphene paper was investigated by scanning electron microscopy (SEM). Figure 1d shows the typical SEM images of graphene paper before and after laser treatment with 50% laser intensity. The pristine graphene paper shows a relatively smooth surface. In contrast, the engineered graphene paper possesses a very rough surface with ordered concaves and convexes. The periodic concaves have a uniform distance of ~30 μm, consistent with the spot size of the laser beam. Such a rough surface may be responsible for enhanced light absorbance and diffuse reflection, leading to the dark colour of the engineered graphene paper. The contact angle (CA) of graphene paper was measured (inset of Figure 1d) and used as the quantitative indicator of changing surface hydrophobicity. The CA of the untreated graphene paper is 30°, which increases dramatically to 131° for the engineered paper, indicative of enhanced surface hydrophobicity. Due to the high surface tension, a water droplet tends to minimize the surface. Although the surface of a hydrophobic substrate is covered with an aqueous solution, the area between ridges on the rough surface may not be filled by the liquid, leading to the formation of a composite interface. As a result, air bubbles are entrapped into micro-/nano-sized pores at the solid surface, where a mix of solid–liquid and solid–gas interfaces is created. Compared to the plain graphene paper, engineered graphene paper with enhanced surface roughness increases the volume of air bubbles entrapped in the interface and the extent of solid–gas interface is proportional to the degree of hydrophobicity of the material[26–28]. Meanwhile, after the laser treatment, the electrical resistance of the paper is reduced from 1.5 to 0.3 kΩ/cm. The enhanced electrical conductivity is attributed to the elimination of oxygen atoms caused by the laser irradiation process (the oxygen atomic content reduced from 19.5% to 14.1% after laser treatment according to the X-ray photoelectron spectroscopy in Figure S2), a phenomenon consistent with previous literatures[2,3]. The changes in surface chemistry and the introduction of surface roughness at the micro-/nano-scale (see also details in Figure 2) by the laser irradiation may both contribute to the enhanced hydrophobicity of engineered graphene papers.

To clarify the effects of laser irradiation intensity, a series of testing samples were prepared under different laser intensities (0%, 10%, 30% and 50%). For the untreated graphene paper (Figure 2a and 2e), the
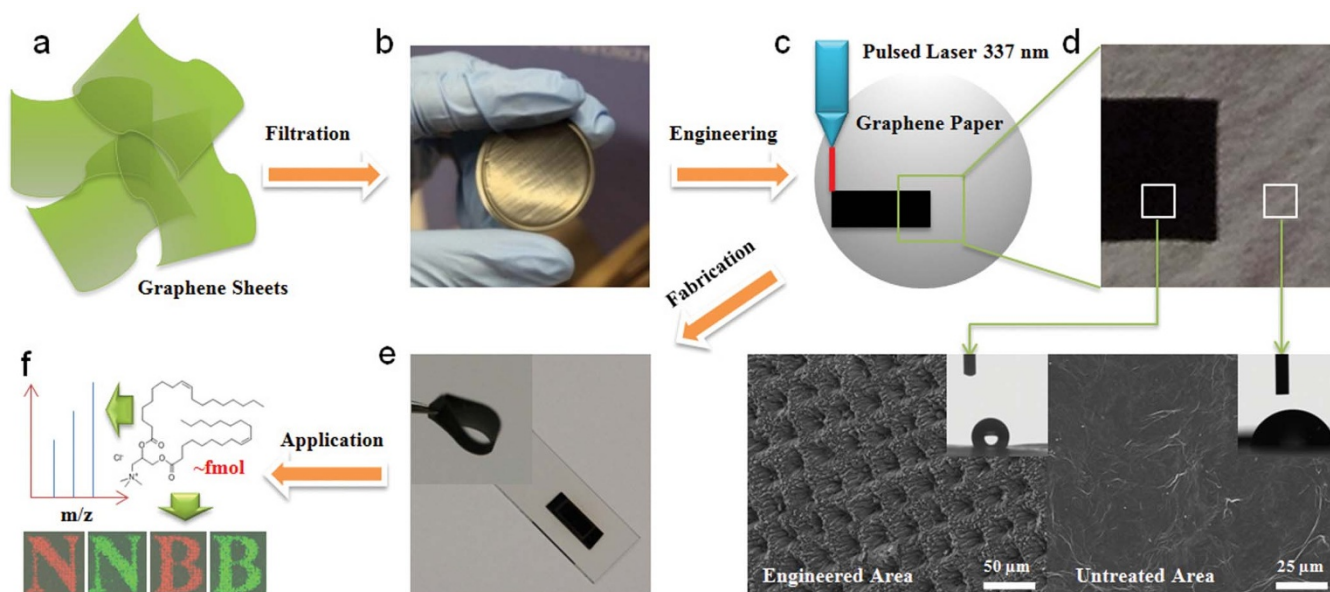

Figure 1 | Schematics of laser engineered graphene paper as a substrate for matrix-free LDI MS detection and imaging of trace amount molecules. (a) The graphene sheets obtained by reduction of graphene oxide. (b) A digital image of the graphene paper obtained by filtration of graphene sheets. (c) The graphene paper is engineered by pulsed laser irradiation in a selected area. (d) The engineered area (darker black) and untreated area show rough and smooth surface, high and low contact angle, respectively. (e) Digital images of the engineered paper after fabrication, which can be used as a substrate for (f) matrix-free LDI MS detection of trace amount molecules and imaging of stamped micro-patterns.
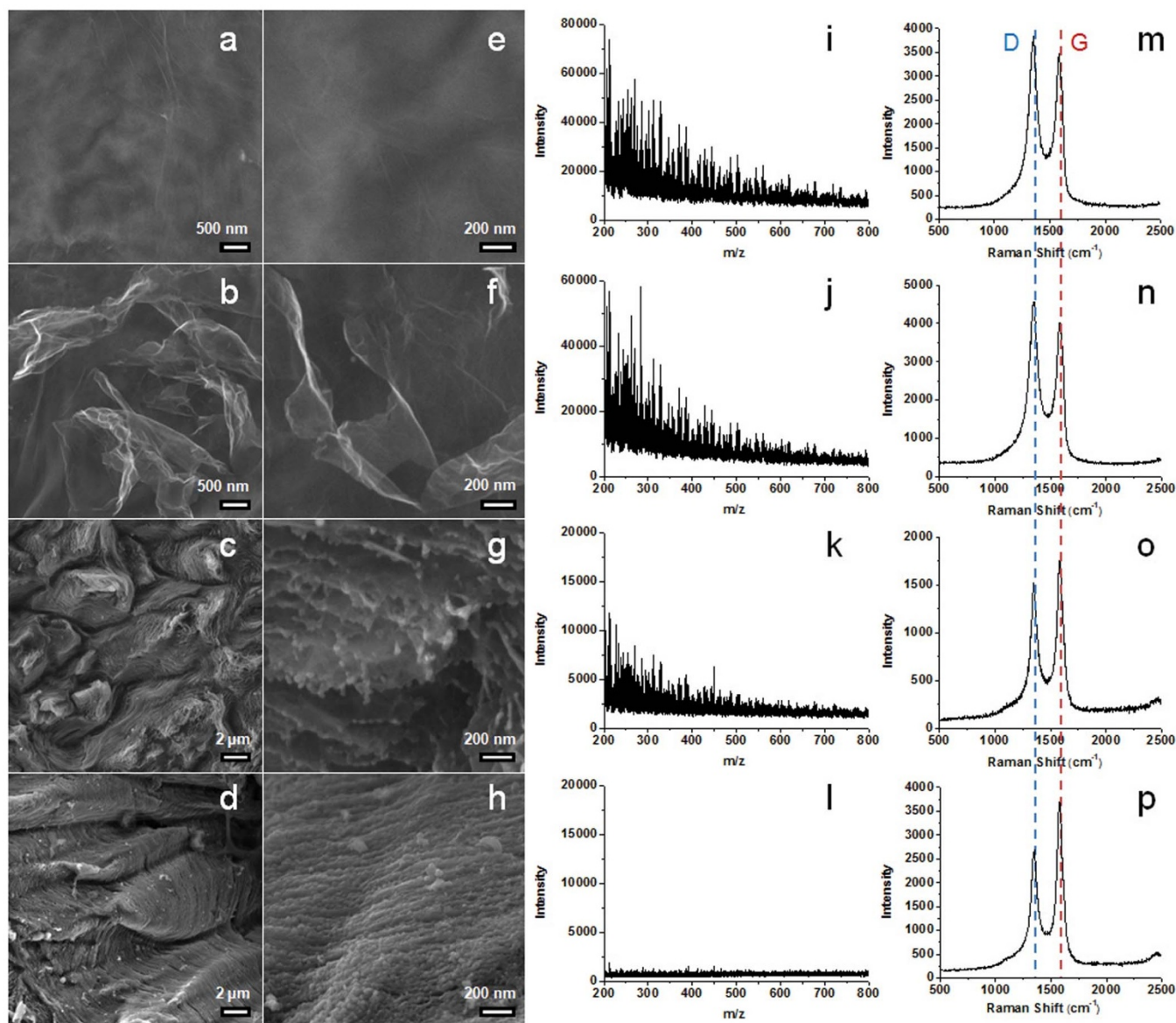
Figure 2 | SEM, MS and Raman characterisation of the graphene paper engineered at different laser intensities. (a, e, i, m) Untreated graphene paper. (b, f, j, n) 10% laser intensity. (c, g, k, o) 30% laser intensity. (d, h, l, p) 50% laser intensity.

graphene sheets are stacked horizontally with very few minor wrinkles found on the surface. Under mild laser irradiation (laser intensity of 10%), the loosely packed graphene sheets on the paper surface begin to peel off and the edges of the exfoliated graphene sheets are exposed to the surface (Figure 2b and 2f). At a laser intensity of 30%, the surface of the paper is dominated by the edges of graphene sheets, indicating that the graphene sheets are no longer parallel to the paper plane (Figure 2c). The ordered array of concaves and convexes can be formed when the laser intensity is reached to 50% (Figure 2d). The morphology of graphene paper under different laser intensity can also be observed in a large scale under lower magnification SEM images as displayed in Figure S3.

Under higher magnification (Figure 2g), nanospheres with sizes of 20–80 nm are observed at the edges of the exfoliated graphene sheets. Further increase of the laser intensity to 50% (Figure 2d, 2h and 3a) leads to the formation of nanospheres arrays on the surface. The surface of the engineered area is fully decorated with aligned nanospheres, which is different from the morphology of laser-engineered graphene with exfoliated layers described in the previous literatures[2,3]. Transmission electron microscopy (TEM) is also used to

investigate the structure of nanospheres, where densely stacked spherical structures can be found on the edge of engineered graphene (Figure 3b). The typical graphitic interlayer spacings ($\sim$0.35 nm) can be clearly observed in the shell (inset of Figure 3b). It was reported that graphene was not stable under electron beam at an acceleration voltage of 80 kV[16,17]. In our experiments, it was noticed that the carbon nanospheres formed on the graphene surface maintained a stable structure under 300 keV electron beam, indicating enhanced stability over bare graphene paper. The engineered paper keeps its unique surface morphology even after sonication (Figure S4a), indicating that the *in situ* grown nanospheres attach firmly to the surface (Figure S4b) and the engineered paper is robust for further applications. The carefully chosen laser engineering parameters in our experiments, including the spot size and spot-spot distance, multiple shots (500) on one spot, high energy laser with a short wavelength with optimised intensity, all favour a fully functionalised, stable and homogenous surface.

The stability of the pristine and engineered graphene papers was examined under LDI MS. As shown in Figure 2i and 2j, both the untreated and mildly engineered (with 10% laser intensity) graphene
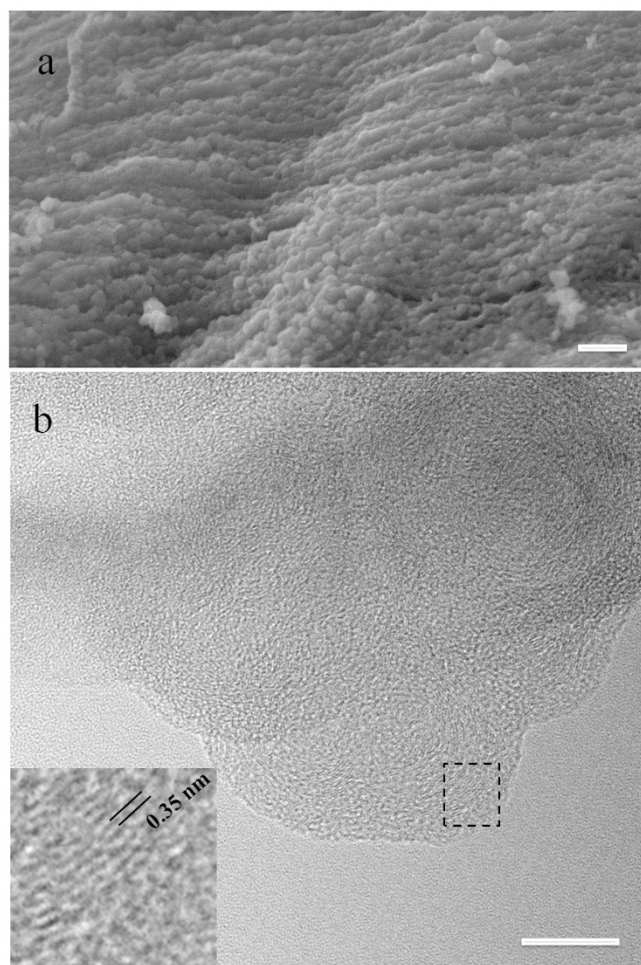
Figure 3 | SEM and TEM images of the nanospheres on the engineered graphene paper. (a) is the high resolution SEM image of the nanospheres in Fig. 2h and the scale bar is 100 nm. (b) is obtained under 300 keV electron beam and the scale bar is 10 nm. The high resolution image of the circled area in b is shown as the inset.

papers produced a large number of fragments from the carbon clusters with signal intensity up to 75,000. In the case of engineered paper with 30% laser intensity (Figure 2k), the fragments can still be observed but with a decreased signal intensity (12,000). The engineered paper with 50% laser intensity produces fragments with significantly lower signal intensity ($< 2,000$, Figure 2l). We conclude that the engineered graphene paper has enhanced stability against fragmentation under laser irradiation compared to the pristine paper by at least two orders of magnitude.

To investigate the origin of the enhanced stability of engineered paper against fragmentation, Raman spectrometry was employed. As shown in Figure 2m–p, all the graphene papers show characteristic peaks for the D, G bands. The I(D)/I(G) ratio is 1.42 for the pristine graphene paper (Figure 2m), which slightly increases to 1.62 (Figure 2n) after irradiated with laser intensity of 10%. The stacked graphene sheets in the pristine paper are slightly damaged and exfoliated (Figure 2b and 2f); as a result, more lattice defects are created and more dangling bonds are exposed, leading to a higher I(D)/I(G) ratio[29,30]. When the laser intensity is increased to 30% and 50%, the I(D)/I(G) ratio is reduced to 0.99 and 0.81, respectively (Figure 2o and 2p), suggesting that the number of lattice defects is decreased with the increase in irradiation energy. It has been reported that carbon atoms at the defect sites are less stable than those located at regular carbon positions[14,15]. With the

reduction in the number of defect carbon atoms and the formation of nanospheres with the increased laser intensity, the stability of engineered graphene paper against further fragmentation can be enhanced.

Taking the advantages of the enhanced stability, hydrophobicity and conductivity, the graphene paper engineered at 50% laser intensity was employed as a substrate for matrix-free MS detection and imaging applications. The performance of the engineered graphene paper is compared with a commercial product, NALDI™ plate (Bruker)[23], for matrix free MS analysis of a small dye molecule acridine orange 10-nonyl bromide (AONB). In the case of the NALDI™ plate, only weak signals of AONB (8.5 fmol) at m/z of 392 $[C_{26}H_{38}BrN_3\text{-}Br]^+$ were observed with signal strength less than 1000 (Figure 4a), whereas on the engineered graphene paper the molecular ion peak was observed with signal strength over 100,000 (Figure 4b), ~100 times stronger compared with that observed on the commercial plate. When the amount of AONB is decreased to less than 1 fmol (0.85 fmol), the analyte signal failed to be identified on the commercial NALDI™ plate (Figure S5a), but was clearly observed on the engineered graphene paper (Figure S5b). It is noted that in control experiments with CHCA used as matrix, weak signals of AONB (8.5 fmol, Figure S6a) can be viewed in the presence of strong CHCA interference peaks and detection fails with decreased AONB amount (0.85 fmol, Figure S6b). It is concluded that the engineered graphene paper has superior performance compared to the commercial product for advanced matrix-free MS applications.

The potential of engineered graphene paper was further demonstrated in MS detection and imaging of lipid molecules. Figure 3c & d showed the MS spectra of a lipid molecule, N-[1-(2,3-dioleoyloxy)-propyl]-N,N,N-trimethylammonium chloride (DOTAP), on unmodified and engineered graphene paper, respectively. In the case of unmodified graphene paper, the signals from DOTAP cannot be identified due to the strong background noise (Figure 4c). In contrast, the background noise is significantly reduced in the case of the engineered paper, and two peaks with strong intensity at m/z of 662 $([C_{42}H_{80}NO_4]^+)$ and 380 $([C_{42}H_{80}NO_4\text{-}C_{18}H_{33}O_2]^+)$ are observed (Figure 4d). The DOTAP signal can be detected on the engineered paper at 30 fmol lipids (Figure S7). For comparison, the matrix-assisted approach using CHCA yields very strong background signals in the spectrum due to matrix fragmentation and can not identify the lipid at low concentrations (see Figure S6c, d). The engineered graphene paper was also successfully applied to the matrix-free detection of two phosphorous lipids (dipalmitoyl-phosphatidyl-choline, DPPC, and hydrogenated soy phosphatidylcholine, HSPC) and the detection of limit reached femtomolar level (Figure S8). The detection of lipids on the engineered graphene paper shows an increase of ~1000 fold, compared to literature reports using graphene based devices (~nmol)[11]. The above results demonstrate the remarkable ionization/detection performance of engineered graphene paper towards various lipid molecules.

To show the matrix-free MS imaging capability of the engineered graphene paper, a stamp was made by laser engraving several letters, where the finest width of letter strokes, e.g., N, is ~150 μm, similar to the typical spatial resolution of a fingerprint. A dilute solution of DOTAP (1.4 pmol/μL) was used as invisible 'ink' for stamping. The stamp was dipped into the solution and then pressed onto the graphene paper to mark the pattern of letters, which is invisible on the stamped paper (Figure S9) and can only be subsequently constructed by 2D matrix-free MS imaging technique (see Methods for details). As indicated in Figure 3d, the signals of DOTAP at m/z of 662 and 380 are monitored and shown in red and green, respectively. The pixel size is 50 μm by 50 μm to distinguish the finest width of letters in the stamp. In the case of un-modified graphene paper, the pattern of stamp is non-resolved and difficult to fully image ('N' in Figure 4e & f, 'A' and 'B' in Figure S10a, b, e, f). In contrast,
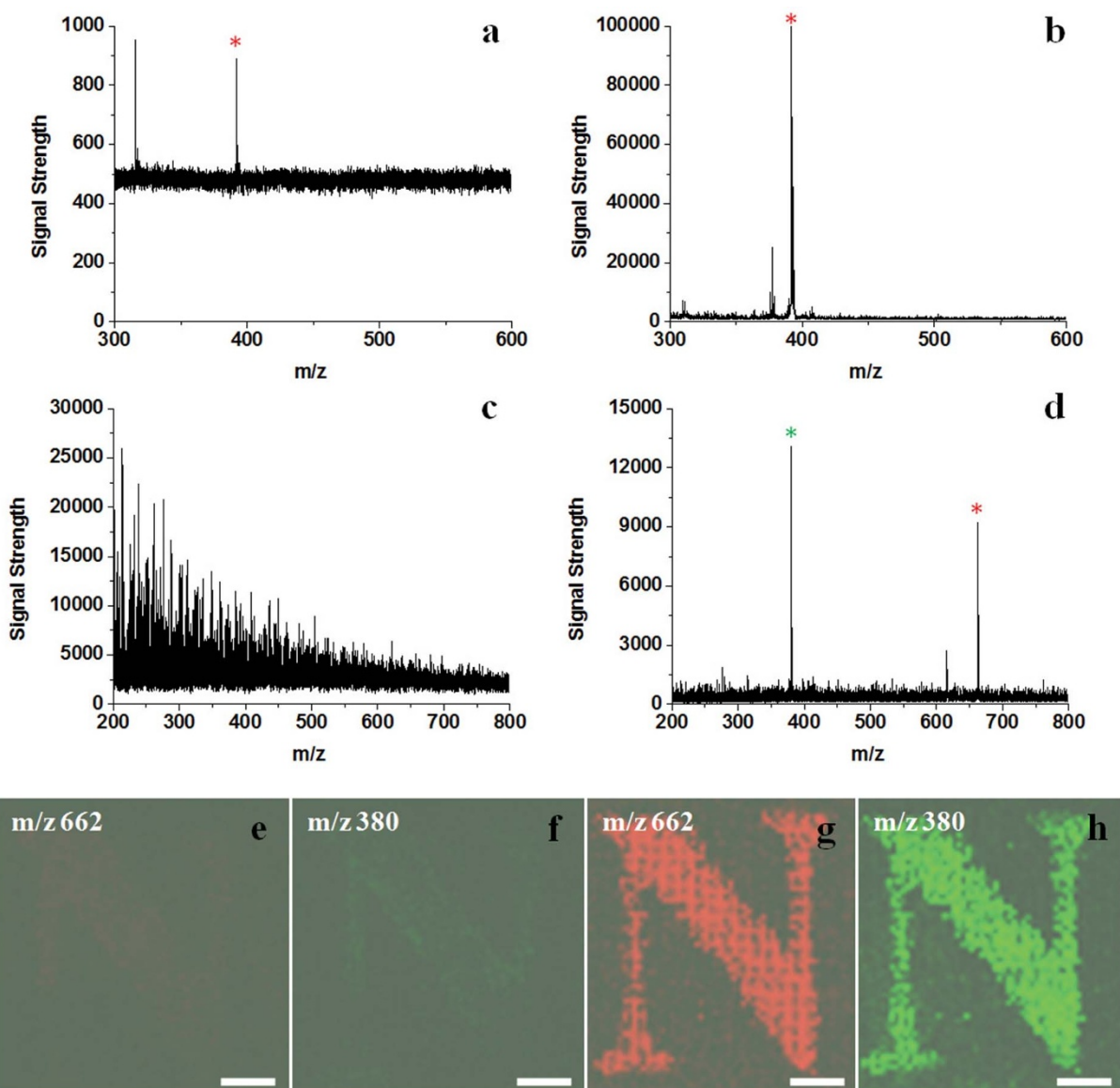
4

Figure 4 | Matrix-free LDI MS detection and imaging of molecules. MS spectra of 8.5 fmol AONB on (a) commercial NALDI™ substrate and (b) engineered graphene paper. MS spectra of 300 fmol DOTAP on (c) untreated graphene paper and (d) engineered graphene paper. MS imaging patterns of a letter 'N' at m/z of 662 and 380 on (e, f) untreated graphene paper and (g, h) engineered graphene paper, respectively. Asterisks indicate the identified ions from the target molecules. The scale bar in e–h is 500 μm.

when the engineered graphene paper is used as the substrate, the pattern of the letters is clear and fully resolved (Figure 4g & h, Figure S10c, d, g, h). It is noted that due to the low concentration (~pmol/μL) and detection of limit (~fmol) for detection and imaging achieved in our study, the engineered graphene paper can be applied not only with tissue blotting for small metabolites and lipids molecules[8,22–25], but also used in the forensic study to track trace amount of chemicals (normal concentration ~nmol/μL, such as drugs) in the latent fingerprint[1,2,9] and record/monitor the invisible micro-pattern of specific molecules.

Discussion

The high performance in matrix-free MS detection and imaging applications can be attributed to the unique structural features of the engineered graphene paper and the improved LDI efficiency of the analytes. The enhanced stability of engineered graphene paper due to decreased defects and the formation of stable graphitic nanosphere arrays effectively prevent the substrate material from unwanted fragmentation and laser energy loss, leading to the ultrahigh ionization/detection efficiency and improved detection sensitivity. Meanwhile, the enhanced surface hydrophobicity can provide strengthened hydrophobic interaction with hydrophobic analyte molecules (such as lipids in our case), favourable for the laser energy transfer to the lipid molecules and for laser induced desorption process[18,31]. The improved electrical conductivity is also beneficial during the LDI process, providing improved electron mobility on the substrate surface for better analyte ionization. Most importantly, the carefully adjusted laser engineering parameters create a homogeneous functional surface, which is crucial for the reliable and high-resolution replication of invisible micro-pattern of low concentration analytes.

In conclusion, we have successfully developed a pulsed laser engineering method to prepare functional graphene-based papers, which have enhanced stability and superior performance in matrix-free MS detection and imaging of a variety of small molecules compared to expensive commercial products. Our contribution is not

only in materials synthesis and fabrication, but also has great potential in diverse applications such as diagnostics, biomarker discovery, and forensic applications.

Methods

Engineering the graphene paper and characterization. In the laser engineering of the obtained graphene paper, the pulsed nitrogen laser with wavelength of 337 nm (200 Hz) was used in the Bruker Autoflex III MS chamber and the paper was loaded on the MALDI plate for further engineering. The imaging mode was employed for the laser engineering, where the spot-to-spot distance is set to be 30 μm and 500 shots were taken at each spot. The laser power was about 121.8 μJ for 100% laser intensity[14]. The laser intensity was set to be 10%, 30% and 50% to get different engineered graphene paper. The engineered paper was tailored into different shapes for mass spectrometry detection and imaging. The SEM images were taken on the JSM-7800F Thermal Field Emission Scanning Electron Microscope, the samples were loaded on the carbon adhesive and baked overnight at 70°C before SEM analysis without coating of gold or platinum. Contact angle measurement was performed by Dataphysics OCA 20-sessible/pendant drop measurement, where 5 μL of water droplet was placed on the substrate paper. X-ray photoelectron spectroscopy analysis was performed on the Kratos Axis Ultra photoelectron spectrometer which used Al K_α (1253.6 eV) X-rays. The electrical resistance of paper was measured using the CM2700 device from the CALTEK instrument. TEM images were taken with a JEOL 2011 microscope operated at 300 kV. The LDI MS spectra of the paper were collected at the laser intensity of 36%, where 500 shoots were taken at 10 spots (50 shots for each spot). The Raman spectra were recorded using 514 nm laser on the Renishaw inVia Raman spectrometer, where mild laser intensity (10%) was used to avoid the further damage to the samples.

Matrix-free LDI MS detection and imaging. The lipid molecules were initially dissolved in chloroform and ethanol was used for AONB at a concentration of 1 mg/mL and then diluted in a step wise manner. To perform to MS detection, typically 0.4 μL of the diluted solution was directly deposited on the paper or NALDI™ plate (Bruker Daltonics), for MS analysis on Bruker Autoflex TOF/TOF III Smartbeam. For the standard matrix assisted detection, 0.4 μL of sample solution was mixed with 1 μL of CHCA matrix (10 mg/mL, in acetonitrile/water/trifluoroacetic acid, 50 : 49.9 : 0.1%, v/v/v) and dried on the commercial MALDI plate (MPT 384 plain steel) before MS analysis. All mass spectra were obtained in the RP-HPC-Proteomics mode via an accumulation of 500 laser shots under a laser intensity of 36% for data collection and calibrated using an auto calibration method. Two standard peptides, Angiotensin II (M.W. 1046.5) and ACTH-Clip (M.W. 2465.7), were used for calibration to reduce variability. No smoothing of spectra was applied. In the imaging experiments, the stamp with laser engraved letters pattern was first fabricated and immersed into a DOTAP solution at a concentration of 1 ng/μL. The stamp was pressed to the paper substrate separately and then the stamped paper was loaded into the MS chamber for imaging. Matrix-free mass spectrometry imaging was performed on the Bruker Autoflex TOF/TOF III mass analyzer system in positive reflector mode. In the imaging set up, the spot-to-spot distance was set to be 50 μm and 50 laser shots were taken with laser intensity of 36% at each spot. The nitrogen laser (337 nm) was applied at a repetition rate of 200 Hz. A full mass spectrum ranging from 200 to 2000 *m/z* was acquired for every pixel at an x-y step-size of 50 μm. Imaging data was stored in the FlexImaging data format (Bruker Bioscience). 2D image construction and statistical analysis were executed using custom-made scripts in the FlexImaging software (Bruker Bioscience, AUS). Peak finding and integration was performed for each pixel to select peaks at specific *m/z* of 380 and 662. Peaks were integrated using a 0.3 Da window.

Received and accepted dates.

1. Novoselov, K. S. *et al.* Electric field effect in atomically thin carbon films. *Science* **306**, 666–669 (2004).
2. Gao, W. *et al.* Direct laser writing of micro-supercapacitors on hydrated graphite oxide films. *Nat. Nanotechnol.* **6**, 496–500 (2011).
3. El-Kady, M. F., Strong, V., Dubin, S. & Kaner, R. B. Laser Scribing of High-Performance and Flexible Graphene-Based Electrochemical Capacitors. *Science* **335**, 1326–1330 (2012).
4. Lim, G. K. *et al.* Giant broadband nonlinear optical absorption response in dispersed graphene single sheets. *Nat. Photonics* **5**, 554–560 (2011).
5. Lim, A. Y., Ma, J. & Boey, Y. C. F. Development of Nanomaterials for SALDI-MS Analysis in Forensics. *Adv. Mater.* **24**, 4211–4216 (2012).
6. Chiang, C. K., Chen, W. T. & Chang, H. T. Nanoparticle-based mass spectrometry for the analysis of biomolecules. *Chem. Soc. Rev.* **40**, 1269–1281 (2011).
7. Northen, T. R. *et al.* Clathrate nanostructures for mass spectrometry. *Nature* **449**, 1033–1036 (2007).
8. Kim, Y. K. *et al.* Synergistic Effect of Graphene Oxide/MWCNT Films in Laser Desorption/Ionization Mass Spectrometry of Small Molecules and Tissue Imaging. *ACS Nano* **5**, 4550–4561 (2011).
9. Dong, X. L., Cheng, J. S., Li, J. H. & Wang, Y. S. Graphene as a Novel Matrix for the Analysis of Small Molecules by MALDI-TOF MS. *Anal. Chem.* **82**, 6208–6214 (2010).
10. Gulbakan, B. *et al.* A Dual Platform for Selective Analyte Enrichment and Ionization in Mass Spectrometry Using Aptamer-Conjugated Graphene Oxide. *J. Am. Chem. Soc.* **132**, 17408–17410 (2010).
11. Lee, J., Kim, Y. K. & Min, D. H. Laser Desorption/Ionization Mass Spectrometric Assay for Phospholipase Activity Based on Graphene Oxide/Carbon Nanotube Double-Layer Films. *J. Am. Chem. Soc.* **132**, 14714–14717 (2010).
12. Tang, L. A. L., Wang, J. Z. & Loh, K. P. Graphene-Based SELDI Probe with Ultrahigh Extraction and Sensitivity for DNA Oligomer. *J. Am. Chem. Soc.* **132**, 10976–10977 (2010).
13. Lu, M. H., Lai, Y. Q., Chen, G. N. & Cai, Z. W. Matrix Interference-Free Method for the Analysis of Small Molecules by Using Negative Ion Laser Desorption/Ionization on Graphene Flakes. *Anal. Chem.* **83**, 3161–3169 (2011).
14. Lu, M. H., Lai, Y. Q., Chen, G. N. & Cai, Z. W. Laser desorption/ionization on the layer of graphene nanoparticles coupled with mass spectrometry for characterization of polymers. *Chem. Commun.* **47**, 12807–12809 (2011).
15. Kawasaki, H. *et al.* Functionalized Graphene-Coated Cobalt Nanoparticles for Highly Efficient Surface-Assisted Laser Desorption/Ionization Mass Spectrometry Analysis. *Anal. Chem.* **84**, 9268–9275 (2012).
16. Warner, J. H. *et al.* Structural transformations in graphene studied with high spatial and temporal resolution. *Nat. Nanotechnol.* **4**, 500–504 (2009).
17. Chuvilin, A., Kaiser, U., Bichoutskaia, E., Besley, N. A. & Khlobystov, A. N. Direct transformation of graphene to fullerene. *Nat. Chem.* **2**, 450–453 (2010).
18. Arakawa, R. & Kawasaki, H. Functionalized Nanoparticles and Nanostructured Surfaces for Surface-Assisted Laser Desorption/Ionization Mass Spectrometry. *Anal. Sci.* **26**, 1229–1240 (2010).
19. Kong, X. L., Li, S. Q., Zhang, S., Huang, Y. & Cheng, Y. S. Large Carbon Cluster Anions Generated by Laser Ablation of Graphene. *J. Am. Soc. Mass Spectrom.* **22**, 2033–2041 (2011).
20. Robertson, A. W. *et al.* Spatial control of defect creation in graphene at the nanoscale. *Nat. Commun.* **3**, 1144 (2012).
21. Bendall, S. C. & Nolan, G. P. From single cells to deep phenotypes in cancer. *Nat. Biotechnol.* **30**, 639–647 (2012).
22. Ifa, D. R., Manicke, N. E., Dill, A. L. & Cooks, G. Latent fingerprint chemical imaging by mass spectrometry. *Science* **321**, 805–805 (2008).
23. Vidova, V. *et al.* Laser Desorption-Ionization of Lipid Transfers: Tissue Mass Spectrometry Imaging without MALDI Matrix. *Anal. Chem.* **82**, 4994–4997 (2010).
24. Steinhauser, M. L. *et al.* Multi-isotope imaging mass spectrometry quantifies stem cell division and metabolism. *Nature* **481**, 516–519 (2012).
25. Zhang, D. S. *et al.* Multi-isotope imaging mass spectrometry reveals slow protein turnover in hair-cell stereocilia. *Nature* **481**, 520–524 (2012).
26. Peng, M., Kurokawa, T., Gong, J. P., Osada, Y. & Zheng, Q. Effect of surface roughness of hydrophobic substrate on heterogeneous polymerization of hydrogels. *J. Phys. Chem. B* **106**, 3073–3081 (2002).
27. Zhang, H., Lamb, R. & Lewis, J. Engineering nanoscale roughness on hydrophobic surface - preliminary assessment of fouling behaviour. *Sci. Technol. Adv. Mater.* **6**, 236–239 (2005).
28. Deng, X. *et al.* Transparent, Thermally Stable and Mechanically Robust Superhydrophobic Surfaces Made from Porous Silica Capsules. *Adv. Mater.* **23**, 2962–2965 (2011).
29. Ferrari, A. C. Raman spectroscopy of graphene and graphite: Disorder, electron-phonon coupling, doping and nonadiabatic effects. *Solid State Commun.* **143**, 47–57 (2007).
30. Cancado, L. G. *et al.* Quantifying Defects in Graphene via Raman Spectroscopy at Different Excitation Energies. *Nano Lett.* **11**, 3190–3196 (2011).
31. Liu, Y., Liu, J. Y., Deng, C. H. & Zhang, X. M. Graphene and graphene oxide: two ideal choices for the enrichment and ionization of long-chain fatty acids free from matrix-assisted laser desorption/ionization matrix interference. *Rapid Commun. Mass Spectrom.* **25**, 3223–3234 (2011).

Author contributions

K.Q. did the experiments, performed the data analysis and wrote the paper. L.Z. and J.L. helped revise the paper. J.Y. performed the transmission electron microscopy. H.X. performed scanning electron microscopy and recorded digital images of the paper. M.Y. helped prepare the stamp. A.N. helped with MS imaging and software set-up. J.Z. helped conduct Raman/SEM/TEM analysis and revise the paper. M.M. helped perform mass spectrometry tests/analysis and revise the paper. C.Y. designed the study with K.Q. and helped write the paper. All the authors discussed the results and commented on the manuscript.

Additional information

Supplementary information accompanies this paper at http://www.nature.com/scientificreports